PHYSICAL REVIEW B VOLUME 8, NUMBER 2 15 JULY 1973

Further Measurements and Calculations of the Far-Infrared Anharmonic Optical Properties of KI between 12 and 300 °K*

J. E. Eldridge and K. A. Kembry
Department of Physics, The University of British Columbia, Vancouver, British Columbia, Canada
(Received 27 February 1973)

Measurements and calculations of the far-infrared optical properties of $K^{39}I$ at 300, 77, and 12 °K are presented. The measurements are mainly those of absorption in crystals of various thicknesses. The calculation assumed cubic anharmonicity only, with nearest-neighbor coupling, and the input lattice-dynamical data were obtained from a shell-model program. These data were generated with a wave-vector density of 32 000 points per zone, which was sufficient to give a 2-3-cm^{-1} resolution. The over-all agreement between experiment and theory, in both the intensity and the structure of the spectra, is good. The magnitude of certain calculated features is, however, too large, indicating a need to consider next-nearest-neighbor interactions. Evidence was also found for three-phonon damping, both beyond the two-phonon limit at all temperatures and at $\bar{\nu}_0$ by 300 °K. From these measurements it was possible to calculate portions of the three-phonon damping spectra, which were found to be reasonable. The higher-phonon effects at 300 °K did not seem noticeably more pronounced than those found in the much harder LiF, and arguments are presented to understand this. Finally, the isotope-induced one-phonon processes which occur in natural KI were calculated. These are shown to be small away from the resonance frequency $\bar{\nu}_0$ and not to be the major damping mechanism at $\bar{\nu}_0$ at low temperatures, in contrast to LiF.

I. INTRODUCTION

Calculations have recently been presented[1] on the far-infrared optical properties of Li^7F and natural LiF, assuming only cubic anharmonicity. The agreement with various experimental data was, in general, good, and there emerged several interesting points which it was felt could be profitably investigated in the case of a different compound of the same structure. One point was that by 300 °K there was evidence of higher-phonon relaxation, arising from quartic anharmonicity, etc., both at high wave numbers, beyond the two-phonon limit, and underneath the main transverse-optic (TO) resonance at $\bar{\nu}_0$ wave number. (The width of the TO resonance peak in the imaginary dielectric constant is proportional to, and the height of the peak inversely proportional to, the damping at $\bar{\nu}_0$.) The reason why these higher-order processes were noticeable in the region of $\bar{\nu}_0$ was due to two factors. First, the calculations showed that relaxation via the creation of two-phonons ("summation" processes) did not occur at $\bar{\nu}_0$ but started at slightly higher wave numbers. Second, the magnitude of the damping by two-phonon "difference" processes was very small at $\bar{\nu}_0$. Above some range of temperatures, proportional to the wave numbers of the phonons involved (through the occupation numbers—see Sec. IV), three-phonon damping will increase more rapidly with temperature than the two-phonon damping. This range of temperatures obviously increases with crystal hardness. In LiF which is one of the hardest alkali halides, 300 °K was sufficient to show the three-phonon damping at $\bar{\nu}_0$. It was thought therefore that in KI, one of the softest rocksalt-structure alkali halides, there may be even greater evidence of three-phonon damping at $\bar{\nu}_0$ by 300 °K. It should be noted here, however, that Berg and Bell[2] have already measured the optical properties of KI at room temperature by the very accurate method of asymmetric Fourier spectroscopy. Comparison with the results of their calculation, which also assumed only cubic anharmonicity, did not markedly show any three-phonon effects in the vicinity of $\bar{\nu}_0$, although there was again the expected high-wave-number tail. This result was to be partly expected since they scaled their calculated values by fitting to the $\bar{\nu}_0$ peak height. We will return to this point again.

A second result of the LiF work was that, as already mentioned, the main resonance was found to relax by two-phonon "difference" processes only (or three-phonon "difference" processes, involving the destruction of at least one phonon), so that as the temperature is lowered, the resonance in Li^7F becomes extremely sharp. In natural LiF, containing 7.5% Li^6, the temperature-independent damping by isotope-induced one-phonon processes was found to limit the sharpness of the resonance at low temperatures, and to account for a large fraction of the $\bar{\nu}_0$ damping up to 300 °K. In KI, however, the ionic mass ratio of iodine to potassium is higher than that for fluorine to lithium, and thus the TO-mode wave number $\bar{\nu}_0$ is higher with respect to the zone-boundary acoustic phonons. Consequently it was expected that relaxation by two-acoustic-phonon summation processes would be

able to occur at $\bar{\nu}_0$, so that no really sharp resonance should occur at low temperatures in pure KI. (Low-energy acoustic phonons do not couple at all strongly due to their long wavelength and similar nature, which in combination produce very small relative displacements of nearest neighbors: Coupling seems to commence at wave vectors approximately halfway across the Brillouin zone.) Natural KI does contain, however, 6.88% K^{41} with the predominant K^{39} so that once again isotope-induced one-phonon damping is present. It was not known how great a part this damping would play at $\bar{\nu}_0$ at low temperatures, nor whether it would become evident in absorption measurements below $\bar{\nu}_0$ where the "difference" damping at low temperatures is small. If this were the case information could be obtained about the phonon eigenvectors at certain symmetry points, as was done for LiF.[3]

A final point to emerge from the LiF work concerned the size and assignment of the two-phonon peaks or features. By performing a lattice summation of the slowly decreasing electronic term in the third derivative of the lattice potential, consideration was given to the magnitude of the cubic coupling by all neighbors. For simplicity, however, the form of the coupling by all neighbors was taken to be the same as that for nearest neighbors. The net result was thought to be an overaccentuation of the calculated spectral features. This work with KI supports this conclusion. With regard to the two-phonon assignments of any features, it was seen that consideration of a few criteria for strong coupling allowed one to predict fairly well which phonons with high-symmetry wave-vector points or branches would combine to produce peaks in the damping spectrum. Investigation of these peaks often showed, however, that large contributions from low-symmetry branches were also present. In the past some careless assignments have been made of these features. The assignments are not inherently of any great importance, but nevertheless are interesting and can be made fairly accurately. Srivastava and Bist[4] have recently analyzed the absorption spectra of KI and NaI. Some time ago Renk[5] reported some very sharp temperature-dependent absorption peaks in KI below $\bar{\nu}_0$ at 5 and 6 °K, which he assigned to specific two-phonon difference processes. The measurements and calculations presented here will resolve some of the claims made in these two communications.

II. DAMPING AND FREQUENCY-SHIFT OF THE TO RESONANCE

The final forms used to compute the frequency-dependent damping (inverse lifetime) $\Gamma(0,j_0;\bar{\nu})$, and frequency shift $\Delta(0,j_0;\bar{\nu})$ of the TO lattice resonant mode, with near-zero wave vector, in rock-salt-structured crystals may be found in Ref. 1. References to the theory underlying these results may also be found there. It may be repeated here that the inclusion of only cubic anharmonicity means that absorption of infrared radiation at any wave number $\bar{\nu}$ occurs through off-resonance excitation of the TO resonance at $\bar{\nu}_0$, which then relaxes to two phonons with equal and opposite wave vector, to give zero final momentum effectively equal to that of the infrared photon, and a combined energy ("summation" or "difference") of wave number $\bar{\nu}$.

The form of $\Gamma(0,j_0;\bar{\nu})$, which will be abbreviated to $\Gamma(\bar{\nu})$, contains the wavevectors, eigenvectors, and eigenvalues of the phonons involved, and the calculation of $\Gamma(\bar{\nu})$ requires a summation over a uniform distribution of wavevectors throughout the Brillouin zone. These lattice-dynamical data were obtained from a shell-model program, using the input parameters of Dolling *et al.*,[6] which they found by fitting to frequency dispersion curves measured at 90 °K by inelastic neutron scattering. Model III was employed,[7] and the data were generated with a wave-vector density of 32 000 points/zone (915 points in the irreducible $\frac{1}{48}$ element of the zone). As a first-order approximation to the temperature-dependent frequency-shifts of the phonons, an over-all 5% frequency reduction, approximately that observed in the TO mode, was applied to produce the 300 °K data. The form of the first, second, and third radial derivatives of the nearest-neighbor potential were again taken as in Ref. 1 where consideration was given to the interaction of all neighbors through the slowly decreasing electronic term. A summation over 50 "shells" of nearest neighbors yielded a constant α'' equal to 3.862 ± 0.002, which modifies the magnitude of the Coulombic terms. These derivatives appear in the cubic-coupling coefficient which in turn is part of $\Gamma(\bar{\nu})$, and their respective magnitudes may be seen in Table I, together with all other input data used in the calculations.

Figure 1 shows the 300 °K calculated $\Gamma(\bar{\nu})$ spectrum, with the difference and summation processes drawn separately, together with the calculation of Berg and Bell, in which the two processes have been combined. In the present calculation with 915 independent wave-vector points, the spectrum was smoothed by convolution with a nine-point least-squares-fitting function,[10] giving a resolution of 2 or 3 cm^{-1}. No hand smoothing has been performed. This resolution explains in part the differences between the two calculations (e.g., the heights and widths of the 142- and 153-cm^{-1} peaks), since the Berg–Bell calculation was performed with only 48 independent wave vectors. Other dissimilarities occur due to the different values of potential derivatives used in the calculations. A fairly important result of this will be seen in the subsection of this section.

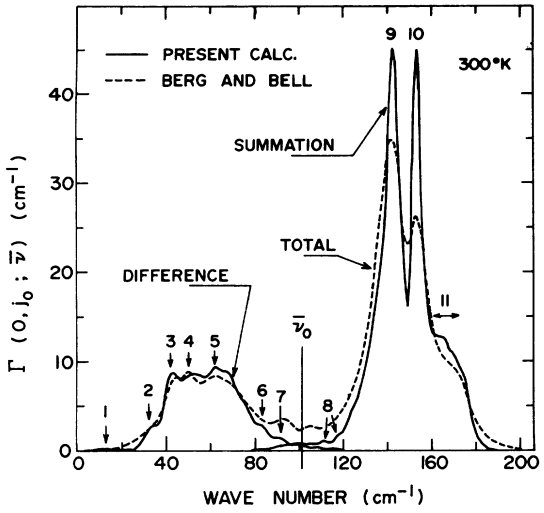

FIG. 1. Present calculation of the two-phonon damping of the TO resonance of $K^{39}I$ at 300 °K, with both processes shown separately (solid lines) and the features labeled; together with the calculation of Ref. 2 with both processes combined (dashed line).

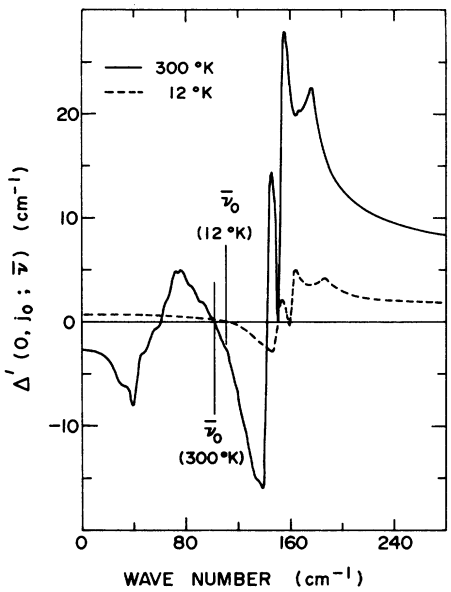

FIG. 2. Calculated frequency-dependent frequency shift of the TO resonance of $K^{39}I$ resulting from two-phonon damping, at 300 and 12 °K. $\bar{\nu}_0$ is the observed resonance wave number.

Figure 2 shows the 300 and 12 °K frequency shifts $\Delta'(\bar{\nu})$ calculated from $\Gamma(\bar{\nu})$ as described in Ref. 1 and adjusted to equal zero at the observed resonance frequency $\bar{\nu}_0$.

Figure 3 shows the 12 °K $\Gamma(\bar{\nu})$ spectra for the sum and difference processes (note the scale change at 120 cm^{-1}) together with the damping of the TO mode due to isotope-induced one-phonon processes, $\Gamma_{iso}(\bar{\nu})$, calculated as described in Ref. 1. The peak near $\bar{\nu}_0$ in $\Gamma_{iso}(\bar{\nu})$ is due to the TO modes across the zone, and the disappearance at 95 cm^{-1} follows from the presence of a band gap which extends down to 69 cm^{-1}. Below this the small amplitudes of the light K^+ ions in the acoustic modes, together with the large wave-number separation from $\bar{\nu}_0$, the small concentration of the isotopes, and the small mass defect all combine to make $\Gamma_{iso}(\bar{\nu})$ very small. (Note that in LiF[3] and NaCl,[11] where larger effects were observed, not only were

TABLE I. Input data for the calculations.

		300 °K	77 °K	12 °K
TO resonance wave number	$\bar{\nu}_0$ (cm^{-1})	101[a]	107.5[b]	109.5[c]
Static dielectric constant	ϵ_0	5.09[c]	4.78[b]	4.68[c]
High-frequency dielectric constant	ϵ_∞	2.65[c]	2.67[b]	2.68[c]
Lattice constant	r_0 (10^{-8} cm)	3.526[d]	3.501[b]	3.492[d]
Compressibility	β (10^{-12}/bar)	8.54[d]	8.00[b]	7.75[d]
Repulsive overlap potential parameters	C (10^{-40} erg)	45.45	60.20	71.04
	ρ (10^{-8} cm)	0.3495	0.3369	0.3302
Third potential derivative	$\phi'''_{N.T.}(r_0)$ (10^{12} erg cm^{-3})	−3.845	−4.234	−4.449
Coulombic term	$\alpha'' e^2/r_0^4$ (10^{12} erg cm^{-3})	0.576	0.592	0.599
Repulsive term	$Ce^{-r_0/\rho}/\rho^3$ (10^{12} erg cm^{-3})	−4.421	−4.826	−5.048
Second potential derivative	$\phi''_{N.T.}(r_0)/r_0$ (10^{12} erg cm^{-3})	0.246	0.267	0.278
First potential derivative	$\phi'_{N.T.}(r_0)/r_0^2$ (10^{12} erg cm^{-3})	0.053	0.053	0.055
Szigeti effective charge	e^*/e	0.72	0.72	0.73

[a]See Ref. 2. [b]Obtained by interpolation. [c]See Ref. 8. [d]See Ref. 9.

TABLE II. Various reported values of $\Gamma(0, j_0; \bar{\nu}_0)$.

	$\Gamma(0, j_0; \bar{\nu}_0)$ equivalent (cm^{-1})	
Jones *et al.*[a] (expt.)	3.48 (R. T.)	3.025 (4.2 °K)
Dolling *et al.*[b] (theo.)	2.06 (300 °K)	0.183 (5 °K) (isotopically pure)
Berg and Bell[c] (expt.)	~2.4 (R. T.)	
Present results (theo.)	~1.4 (300 °K) (~0.6 Diff + ~0.8 Sum)	0.16 (12 °K) (~0.08 Sum + ~0.08 Isotope)

[a] See Ref. 12. [b] See Ref. 6. [c] See Ref. 2.

there no band gaps, but the mass defect was large in the first case, and the concentration large in the second.) Consequently it appears that little information may be obtained from the isotope-induced absorption away from $\bar{\nu}_0$, but that at $\bar{\nu}_0$ at low temperatures these damping processes will be of approximately equal strength with the two-phonon summation processes.

It is also of interest to compare the various values of resonance damping $\Gamma(0, j_0; \bar{\nu}_0)$ calculated or measured by other authors. Table II lists some of these, and it may be seen that while there is general agreement at room temperature, the one low-temperature experimental value of Jones *et al.* is far larger than the calculated values. Since the measurements by Jones *et al.* were performed on thin films, could this indicate surface-mode relaxation? (Their room-temperature value is also high.)

Two-Phonon Assignments

Criteria for the strong coupling of two phonons have been given.[13] On the basis of these, Table III lists the pairs of high-symmetry phonons which may be expected to produce features in the $\Gamma(\bar{\nu})$ spectrum if the dispersion slopes are matched (parallel for difference, opposite for summation). The approximate reduced-wave-vector position h is given where the slope matching is optimum. Figure 4 shows the dispersion curves resulting from the shell-model calculation, for KI at 90 °K. The Σ_4 curves and those from L through W to X were not measured by neutron scattering. The feature numbers in Fig. 1 and Table III refer to the 300 °K spectrum, with its 5% frequency reduction, whereas the wave numbers in Table III were taken from the 90 °K data of Fig. 4. Some of the strong low-symmetry combinations are also listed in Table III but it was not felt worthwhile to list them all. Of importance also is the energy of the destroyed phonon in the difference processes, as is obvious by 12 °K, where the maximum around 80 cm^{-1} corresponds to the $\Delta_5\Delta_5$ combination (combinations at X are forbidden), since the Δ_5 acoustic mode is the least energetic of all.

TABLE III. Expected maxima in two-symmetry-phonon combinations and feature assignments.

	Difference		Summation	
Symmetries of combining phonons	Wave numbers at, and positions of (h), maximum expected contribution	Corresponding infrared wave number (cm^{-1}) and feature assignment (n) if appropriate	Wave numbers at, and positions of (h), maximum expected contribution	Corresponding infrared wave number (cm^{-1}) and feature assignment (n) if appropriate
$\Delta_1\Delta_1$	111 − 66 (0.6)	45 (small)	114 + 66 (0.6)	180 (11)
$\Delta_5\Delta_5$	109 − 28 (0.7)	81 (6) at 300 °K over-all max at 12 °K	109 + 28 (0.7)	137
$\Sigma_1\Sigma_1$	116 − 65 (0.7)	51 (small)	118 + 66 (0.5)	184 (11)
$\Sigma_4\Sigma_4$	96 − 54 (0.5)	42 (3)	96 + 54 (0.5)	150 (9)
$\Sigma_1(LO)\Sigma_4(TO)$	120 − 96 (0.5)	24 (very small)		>200 (very small)
$\Sigma_1(LO)\Sigma_4(TA)$	116 − 53 (0.6)	63	118 + 54 (0.5)	172 (11)
$\Sigma_1(LA)\Sigma_4(TO)$	96 − 66 (0.5)	30 (2)	96 + 66 (0.5)	162 (10)
$\Sigma_1(LA)\Sigma_4(TA)$	66 − 54 (0.5)	12 (1)	66 + 54 (0.5)	120 (small)
$L_1'L_1$	128 − 69	59	128 + 69	197 (effective two-phonon limit)
$L_1'L_3$	128 − 54	74	128 + 54	182 (11)
$L_3'L_1$	96 − 69	27	96 + 69	165 (10)
$L_3'L_3$	96 − 54	42 (3)	96 + 54	150 (9)
W_1W_2'	104 − 58	46 (3)	104 + 58	162 (10)
$(L_3' \rightarrow W_2') + (L_1 \rightarrow W_1)$ ($A + B$ in Fig. 4)				162 (10)
$\Gamma \rightarrow Q$ and W		4 and 5		

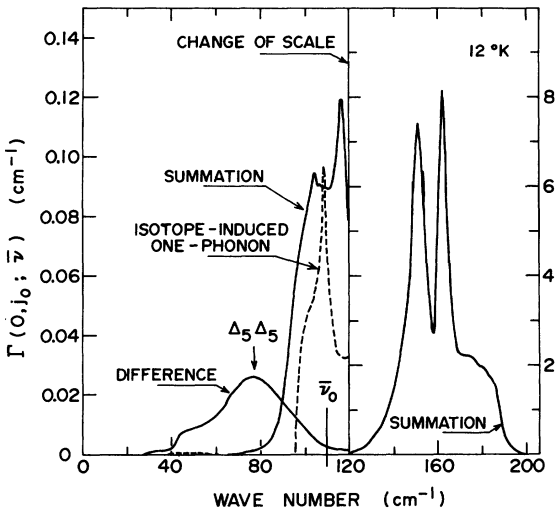

FIG. 3. Calculated two-phonon damping of the TO resonance of $K^{39}I$ at 12 °K via difference and summation processes, drawn separately; together with the isotope-induced one-phonon damping of the resonance in natural KI. The left-hand scale refers to all curves up to 120 cm^{-1}.

Of further interest are the phonon pairs which determine the limits of the two kinds of process. Of importance in this respect is the low coupling obtained between acoustic modes. Not only is there very little coupling between small wave-vector acoustic phonons, as already mentioned, so that combinations do not become significant until halfway to the zone boundary, but even after this no great coupling is obtained. $\Delta_1\Delta_5$ combine only through a term involving the first and second radial derivatives [$\phi'(r_0)$ and $\phi''(r_0)$; see Eq. (6) in Ref. 1] which is typically only 10% of the third derivative $\phi'''(r_0)$ through which major combinations occur. Likewise Σ_3 combines with any other mode in this manner only. Both $\Lambda_1\Lambda_3$ and $\Sigma_1\Sigma_4$ (acoustic) combine through $\theta'''(r_0)$ but only weakly, since the former are forbidden at the zone boundary due to the motion of one ion only, and the latter is small by virtue of the polarization directions involved in the modes. These produce the same kind of relative displacement along a Cartesian direction where the nearest neighbors are located [see Eq. (6) in Ref. 1]. Consequently the lowest difference combinations in LiF were with optic modes ($\Sigma_4\Sigma_4$ and $L_3'L_3$), whereas in KI they are the very weak $\Sigma_4\Sigma_1$ acoustic. Similarly in LiF the first summation pairs were the transverse-optic modes near $\bar{\nu}_0$ with low-energy acoustic modes [just far enough away from the origin for the sine-modulation term in $\Gamma(\bar{\nu})$ to take effect]. These were then necessarily above $\bar{\nu}_0$. Similar combinations are seen as features marked 8 in Fig. 1. In KI, however, where the TO mode is so high, the first summation pairs are the weak acoustic ones with wave vectors approximately halfway across the zone. Thus it may be seen that the magnitudes of $\phi''(r_0)$ and $\phi'(r_0)$ determine to a great extent the summation damping at $\bar{\nu}_0$ in KI, and the difference in $\Gamma(\bar{\nu}_0)$ between the calculated value here and that due to Berg and Bell lies in the different values used for these derivatives.

The high-wave-number limit of the difference processes is simply the highest-energy longitudinal-optic mode near the zone origin, with a low-energy acoustic mode, the intensity decreasing rapidly as the origin is approached. Theoretically the highest summation combination can come from two optic modes, $\Sigma_1\Sigma_4$ for instance, but these are found to be very weak just as were the acoustic combinations, so that the "effective" limit as in LiF may be taken as L_1L_1'.

III. OPTICAL PROPERTIES

The optical properties will be calculated for isotopically pure $K^{39}I$ only, since it has been seen in Fig. 3 that the isotope-induced one-phonon damping has a small effect away from $\bar{\nu}_0$ where the present measurements were performed. It can easily be included in the calculation if in the future low-temperature measurements are performed in the region of $\bar{\nu}_0$ on natural KI. The resonance peak at 12 °K should be approximately only half as sharp in natural KI as in the isotopically pure material.

A. Dielectric Constants

Figure 5 shows the real dielectric constant ϵ' at 300 and 12 °K, calculated as in Ref. 1. Once again the Szigeti effective charge e^* has been calculated by using the measured values of ϵ_0, ϵ_∞, and $\bar{\nu}_0$, and including the "static" frequency shift $\Delta'(0)$ of the

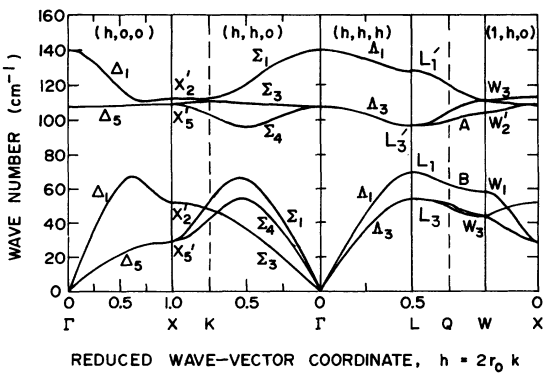

FIG. 4. Frequency dispersion curves of KI along major symmetry directions, generated by the shell model, for KI at 95 °K. The shell model was fitted to neutron measurements, which did not include the Σ_4 modes or those from L through W to X.

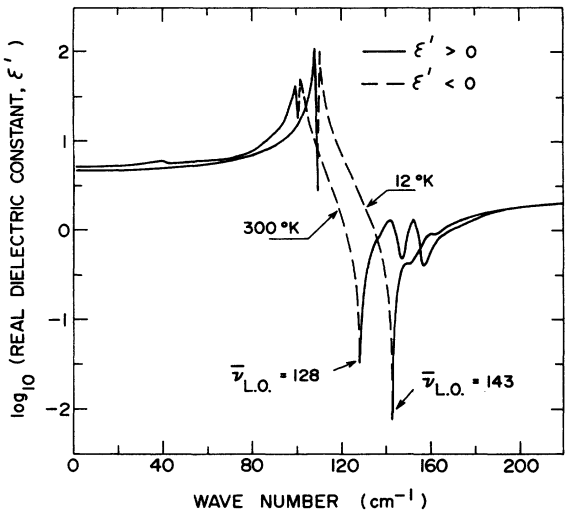

FIG. 5. Calculated real dielectric constants of $K^{39}I$ at 300 and 12 °K. The predicted frequency of the longitudinal-optic mode with near-zero wave vector, $\bar{\nu}_{LO}$, occurs when ϵ' passes through zero.

TO resonance produced by the cubic anharmonicity [see Eq. (25) in Ref. 1]. This latter is the only departure from the usual harmonic approximation used to obtain e^*. With $\Delta'(0)$ equal to -2.7, -0.3, and $+0.7$ cm^{-1} at 300, 77, and 12 °K, respectively, the values of e^* so obtained differ little from the harmonic values[8] and may be found in Table I.

Another departure from harmonicity occurs in the wave number at which ϵ' passes through zero. This is then the predicted wave number of the longitudinal-optic mode with near-zero wave vector, $\bar{\nu}_{LO}$. In the harmonic approximation, the Lyddane-Sachs-Teller (LST) relationship is obtained,

$$\bar{\nu}_{LO}^2/\bar{\nu}_0^2 = \epsilon_0/\epsilon_\infty \ , \tag{1}$$

which with the experimental values in Table I predicts $\bar{\nu}_{LO}$ to be 145 and 140 cm^{-1} at 12 and 300 °K, respectively.

Upon including cubic anharmonicity, Eq. (1) is modified as shown in Ref. 1 to be

$$\frac{\bar{\nu}_{LO}^2}{\bar{\nu}_0^2} = \frac{\epsilon_0}{\epsilon_\infty}\left(1+\frac{2\Delta'(0)}{\bar{\nu}_0}\right)+\frac{2}{\bar{\nu}_0}\left[\Delta'(\bar{\nu}_{LO})-\Delta'(0)\right] . \tag{2}$$

With $\Delta'(\bar{\nu}_{LO})$ equal to -12 cm^{-1} (300 °K) and -2.4 cm^{-1} (12 °K), and the same values of ϵ_0, ϵ_∞, and $\bar{\nu}_0$, Eq. (2) predicts the values of $\bar{\nu}_{LO}$ to be 143 cm^{-1} at 12 °K and 128 cm^{-1} at 300 °K, as shown in Fig. 5.

The only value of $\bar{\nu}_{LO}$ measured by inelastic neutron diffraction is that at 90 °K, equal to 142 cm^{-1}. This does not discriminate between the harmonic and anharmonic 12 °K values of 145 and 143 cm^{-1}, both of which are a little higher as expected.

At 300 °K, the optical measurements of Berg and Bell[2] allow $\bar{\nu}_{LO}$ to be deduced. It may be shown that at $\bar{\nu}_{LO}$, where $\epsilon'=0$, the refractive index n, equals the extinction coefficient k. This occurs in Berg and Bell's data at approximately 129 cm^{-1}, in far better agreement with the anharmonic value of 128 cm^{-1} than the LST value of 140 cm^{-1}. Furthermore, the temperature variation of $\bar{\nu}_{LO}$ as predicted by Eq. (2) is similar to that observed in the resonant mode $\bar{\nu}_0$, whereas the temperature variation in the LST predicted values of $\bar{\nu}_{LO}$ is very small. This gives confidence then in the calculated frequency shifts of Fig. 2.

Figure 6 shows the imaginary dielectric constants, again at 12 and 300 °K. The factor-of-20 reduction in $\Gamma(\bar{\nu}_0)$ in going from 300 to 12 °K is seen most clearly in the ϵ'' resonance peak, whereas it is not so obvious in the related constants n and k (since $\epsilon'' = 2nk$).

B. Absorption Coefficient

The absorption coefficient α from 0 to 300 cm^{-1} was calculated from ϵ' and ϵ'' at 300, 77, and 12 °K and may be seen in Fig. 7. Also shown are the present experimental data obtained at the three temperatures, and the room-temperature data of Ref. 2, converted from k to α. For the sake of clarity the data between 140 and 180 cm^{-1} has been omitted and may be seen in Fig. 8 where the 300 and 77 °K curves have been vertically displaced.

C. Experimental

The measurements were performed on an RIIC. FS720 Fourier spectrometer, with a step drive

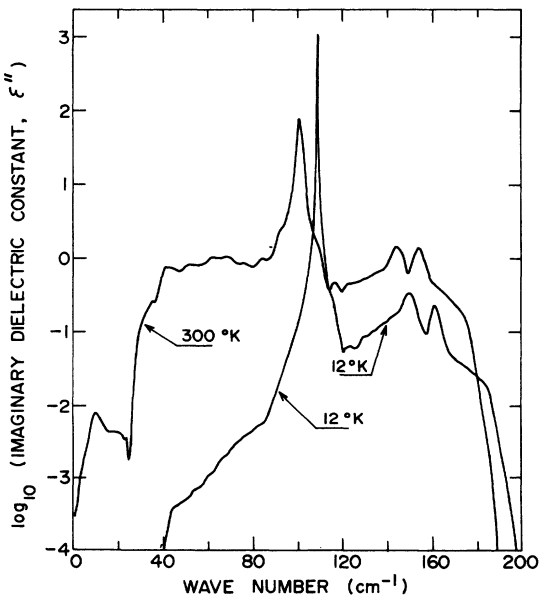

FIG. 6. Calculated imaginary dielectric constants of $K^{39}I$ at 300 and 12 °K.

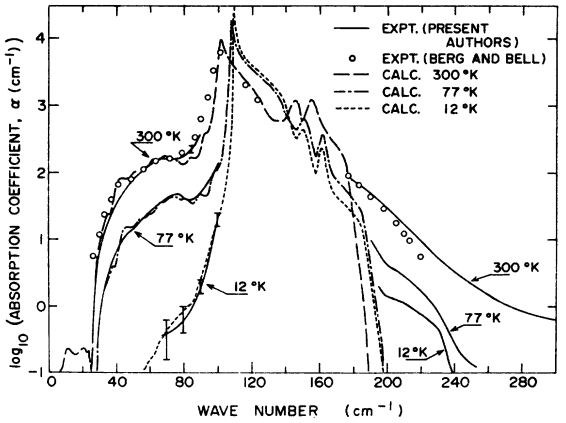

FIG. 7. Present experimental and calculated values of the absorption coefficient of $K^{39}I$ at 300, 77, and 12 °K, together with the room-temperature experimental data from Ref. 2. The experimental data obtained between 140 and 180 cm^{-1} have been omitted for clarity.

and Golay detector. The single crystals of natural KI were obtained from Harshaw Chemical Co. and cleaned and polished to the desired thickness d, which varied from 0.01 to 1.0 cm. A slight wedge shape was produced in order to eliminate interference fringes. They were then ultrasonically cleaned in toluene, rinsed in alcohol, and dried. Transmission measurements of intensity with and without the sample in the beam, I and I_0, respectively, are related by

$$I=\frac{I_0(1-R)^2(1+k^2/n^2)e^{-\alpha d}}{1-R^2e^{-2\alpha d}}\ , \tag{3}$$

where R is the power reflectivity and α the absorption coefficient. Below $\bar{\nu}_0$, it was convenient to correct for R by using the calculated values, which agreed well with experimental values. Above $\bar{\nu}_0$ the measured reflectivity was used. The maximum effect of the $(1+k^2/n^2)$ term in Eq. (3) was about 5% in the region of highest absorption above $\bar{\nu}_0$ at 300 °K, and the effect was negligible elsewhere. The average of several runs was taken with the most reliable data obtained in the region of αd equal to unity. Thus a range of thicknesses was needed. An error bar is shown on the 300 °K data around 80 cm^{-1} and this was typical, although a larger uncertainty should be associated with the highest absorption in Fig. 8 which was at the limit of our signal to noise. The larger bars on the 12 °K data were due to several causes. The first was the low absorption combined with high reflectivity. The second was temperature instability, which has a very marked effect below 90 cm^{-1} where the absorption is due to difference processes. Finally, a peak at 77 cm^{-1} due to small amounts of Cl^- impurity[14] in the Harshaw KI was subtracted out from the data, causing some uncertainty in the remainder.

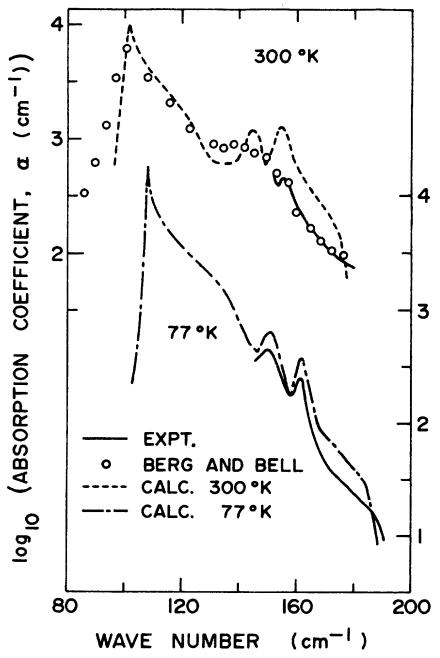

FIG. 8. Present experimental and calculated values of the absorption coefficient of $K^{39}I$ at 300 and 77 °K in the range omitted for clarity from Fig. 7. The room-temperature experimental data from Ref. 2 have been included. The data for each temperature have been vertically displaced, with the ordinate axis and scale for the 77 °K data on the right.

D. Refractive Index and Reflectivity

Figure 9 shows the present calculated values of refractive index together with the 300 °K measured values from Ref. 2. The 300 °K calculated reflec-

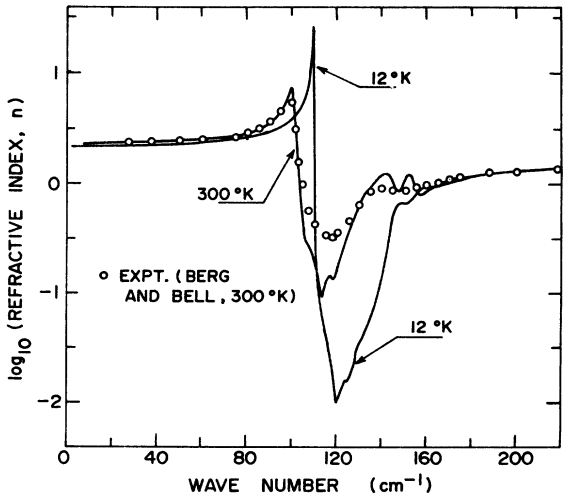

FIG. 9. Calculated refractive indices of $K^{39}I$ at 300 and 12 °K, together with the room-temperature experimental data from Ref. 2.

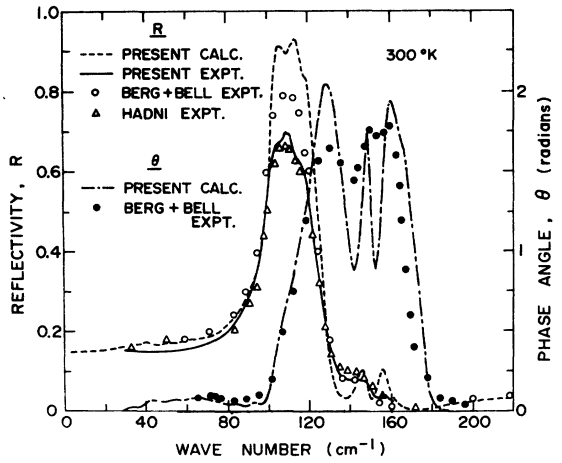

FIG. 10. Calculated 300 °K reflectivity and phase angle of $K^{39}I$. Together with the present experimental reflectivity, the experimental data from Refs. 2 and 14 are presented.

tivity and phase angle are shown in Fig. 10 together with the measurements from Ref. 2, and the reflectivity measured both by ourselves and by Hadni.[15] Both of the power reflectivity measurements agree fairly well but fall below the square-of-the-amplitude measurement of Berg and Bell. This latter measurement is probably the more accurate. We were able to see the two small reflectivity features at 145 and 155 cm^{-1}, not so apparent in the other data. The structure over the peak depended on surface preparation and is probably not a good indication of the $\Gamma(\bar{\nu})$ features in that region (see Fig. 1).

IV. DISCUSSION

A. Three-Phonon Damping

The evidence for three-phonon damping around $\bar{\nu}_0$ at 300 °K may be seen in Fig. 7 (from 80 to 100 cm^{-1}), in Fig. 9 (from 100 to 130 cm^{-1}), and in Fig. 10 (from 100 to 125 cm^{-1}). The more direct evidence of higher-phonon damping is the present set of absorption measurements above the two-phonon limit (from 200 to 300 cm^{-1}) at all three temperatures, seen in Fig. 7. Assuming this is indeed three-phonon (or higher) damping of the TO resonance, and not due to second-order electric moments, then these measurements of α may be converted to damping by means of the relation

$$\alpha(\mathrm{cm}^{-1}) = \frac{4\bar{\nu}_0 e^{*2}(\epsilon_\infty+2)^2(M^+ + M^-)\bar{\nu}\,\Gamma(\bar{\nu})}{9nvc^2M^+M^-\{[\bar{\nu}_0^2-\bar{\nu}^2+2\bar{\nu}_0\Delta'(\bar{\nu})]^2+4\bar{\nu}_0^2\Gamma^2(\bar{\nu})\}}\ , \quad (4)$$

which may be obtained from Eq. (20) in Ref. 1. If $\Gamma(\bar{\nu})$ is removed from the denominator, since its effect will be negligible away from the resonance at $\bar{\nu}_0$, and if the calculated value of refractive index n is used, since this will be fairly accurate beyond 180 cm^{-1}, then Eq. (3) relates $\Gamma(\bar{\nu})$ due to three-phonon (or higher) processes, to the absorption coefficient α measured beyond the two-phonon limit. The values so obtained may be seen in Fig. 11, from 180 cm^{-1} onwards.

The 300 °K values in Fig. 11 between 80 and 130 cm^{-1}, which are responsible for the effects mentioned above, were obtained in an approximate fashion by merely subtracting our values of $\Gamma_{2\text{-phonon}}(\bar{\nu})$ from those of Berg and Bell (see Fig. 1). This was done because the latter authors obtained fairly good agreement between theory and experiment for n and k in the vicinity of $\bar{\nu}_0$. Their agreement followed from their peak-height fitting [which determined their value for $\phi'''(\gamma_0)$] and their larger second and first derivatives, which gave greater values of $\Gamma(\bar{\nu})$ around $\bar{\nu}_0$ as explained in Sec. IIA.

The final resulting 300 °K partial curve of Fig. 11 appears very reasonable, being fairly smooth, and peaking around 160–170 cm^{-1}. This would correspond to the creation of three acoustic phonons from regions near the low-energy critical points (e.g., L_3, Σ_4, or X_2'), which all have wave numbers around 55 cm^{-1}.

It may be noted that, contrary to expectation, the high-wave-number tail and the discrepancy around $\bar{\nu}_0$ in KI does not appear to be noticeably more pronounced than the similar effects found in the much harder LiF. This may be understood by considering the following approximate relations:

$$\Gamma_{2\text{-phonon}}(\bar{\nu}) \propto S(\bar{\nu})_{2\text{-phonon}}/\mu^3\bar{\nu}_1\bar{\nu}_2\bar{\nu}_0\ , \quad (5)$$

$$\Gamma_{3\text{-phonon}}(\bar{\nu}) \propto S(\bar{\nu})_{3\text{-phonon}}/\mu^4\bar{\nu}_1\bar{\nu}_2\bar{\nu}_3\bar{\nu}_0\ , \quad (6)$$

where μ is the reduced mass, $\bar{\nu}_1, \bar{\nu}_2$, and $\bar{\nu}_3$ are the wave numbers of the phonons involved, and $S(\bar{\nu})$ are

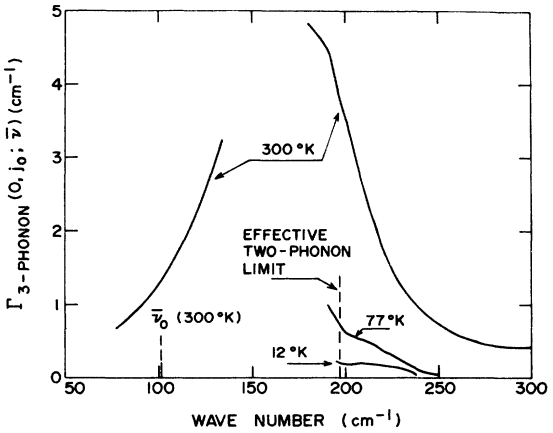

FIG. 11. Portions of the three-phonon (and higher) damping of the TO resonance of $K^{39}I$ at 300, 77, and 12 °K. The methods of obtaining these curves are explained in the text.

terms involving the occupation numbers $n(\vec{k}, j)$ of the phonons. $S(\bar{\nu})_{2\text{-phonon}}$ was fully defined in Ref. 1, but may be given here for the summation processes,

$$S(\bar{\nu})_{2\text{-phonon-summation}} = [n(\vec{k}, j_1) + n(-\vec{k}, j_2) + 1] \times \delta[\bar{\nu} - \bar{\nu}(\vec{k}, j_1) - \bar{\nu}(-\vec{k}, j_2)] , \quad (7)$$

where

$$n(\vec{k}, j) = [e^{h\bar{\nu}(\vec{k}, j)/ck_BT} - 1]^{-1} . \quad (8)$$

The equivalent three-phonon-summation expression is given by

$$S(\bar{\nu})_{3\text{-phonon-summation}} = [n(\vec{k}_1, j_1)n(\vec{k}_2, j_2) + n(\vec{k}_2, j_2)n(\vec{k}_3, j_3) + n(\vec{k}_1, j_1)n(\vec{k}_3, j_3) + n(\vec{k}_1, j_1) + n(\vec{k}_2, j_2) + n(\vec{k}_3, j_3) + 1] \times \delta[\bar{\nu} - \bar{\nu}(\vec{k}_1, j_1) - \bar{\nu}(\vec{k}_2, j_2) - \bar{\nu}(\vec{k}_3, j_3)] \quad (9)$$

and

$$\vec{k}_1 + \vec{k}_2 + \vec{k}_3 = 0 . \quad (10)$$

Equations (5) and (6) do not contain the potential derivatives, which increase rapidly in magnitude with increasing order of derivative, nor any details of the coupling coefficients. The point is that we are concerned with the ratio of $\Gamma_{3\text{-phonon}}(\bar{\nu})/\Gamma_{2\text{-phonon}}(\bar{\nu})$ for different compounds of the same structure, and the variation in the ratio of the factors omitted, from one compound to another, is much smaller than that obtained from the factors present.

The ratio (R for brevity) is then given approximately by

$$R = \frac{\Gamma_{3\text{-phonon}}(\bar{\nu})}{\Gamma_{2\text{-phonon}}(\bar{\nu})} \propto \frac{S(\bar{\nu})_{3\text{-phonon}}}{S(\bar{\nu})_{2\text{-phonon}}\,\mu\bar{\nu}} , \quad (11)$$

where $\bar{\nu}$ is some average or characteristic wave number. R obviously depends on temperature and to some extent on the process, but in the high-temperature limit $S(\bar{\nu})_{3\text{-phonon}}$ approximates to $(ck_BT/h\bar{\nu})^2$, while $S(\bar{\nu})_{2\text{-phonon}}$ approximates to $ck_BT/h\bar{\nu}$. Thus R becomes proportional to $T/\mu\bar{\nu}^2$. In the gross approximation of equal central force constants for all alkali halides, $\mu\bar{\nu}^2$ is constant. Furthermore, the ratio of the damping due to any higher-order process to that due to any other-order process will contain some power of $\mu\bar{\nu}^2$ and may thus be expected to be the same order of magnitude for all compounds of the same structure at high temperatures. A similar situation exists in the ratio of the peak heights of two-phonon damping to the resonance frequency ν_0 at high temperatures, which may be seen to be approximately equal for KI and LiF. This ratio, however, involves $\mu^3\bar{\nu}^5$, and depends much more on the structure of $\Gamma_{2\text{-phonon}}$.

At very low temperatures it is interesting to observe that for the summation processes, $S(\bar{\nu})$ becomes unity and thus R should be even greater for LiF than for KI ($\mu_{LiF}/\mu_{KI} \sim \frac{1}{6}$ and $\bar{\nu}_{LiF}/\bar{\nu}_{KI} \sim 3$). The difference processes, which are the ones responsible for the greater majority of the damping at $\bar{\nu}_0$, are not so straightforward. It may be argued, however, that R will again be approximately constant from one compound to another, since the larger $S(\bar{\nu})_{3\text{-phonon}}$ in the softer compounds will be compensated by the larger μ. R at these low temperatures will of course be very small for the difference processes. Although 300 °K may be considered high for KI but only intermediate for LiF, the general similarity in the 300 °K spectra of KI and LiF may thus be understood.

B. Two-Phonon Damping Structure

It may be seen from Fig. 7 that no distinct features exist in the difference spectrum (below $\bar{\nu}_0$) of KI at any temperatures. The hump around 75 cm^{-1}, prominent at 77 °K, merely reflects the over-all maximum in the difference $\Gamma(\bar{\nu})$, which then decreases strongly until the summation processes start. The sharp features reported by Renk[5] at 5 and 6 °K must therefore be due to impurities. Almost certainly Cl^- would be responsible for the sharp peak at 77 cm^{-1} (trace amounts in our Harshaw sample gave us a similar peak). It is also known[16] that larger concentrations of Cl^- give rise to band structure around 60 cm^{-1}. The temperature variation of the peaks is a little hard to understand, although the two-phonon background is certainly temperature dependent. Nevertheless no sharp peaks can occur in the difference spectrum of any compound at very low temperatures, and in the case of the rocksalt-structured ones, no two-phonon combinations from X, as claimed by Renk, are allowed in any circumstances.

In the summation region, Figs. 8 and 10 show two distinct features. The positions of these agree very well with theory at 77 °K (161 and 150 cm^{-1}) and seem to agree satisfactorily at 300 °K, with the 5% reduction that was applied (155 and 145 cm^{-1}: a slight anharmonic frequency shift is also present). The magnitude of these calculated features, however, together with the "hump" at wave numbers just above them, appears once again to be too large. The coupling, assumed to be between nearest neighbors only, has over accentuated them, and next-nearest-neighbor interactions are necessary. The features in question have been labeled 9, 10, and 11 both in Fig. 1 and in Table III. It may be seen that many strong combinations from nearest-neighbor coupling have by chance contributed to the same peaks. $\Sigma_4\Sigma_4$ and $L_3'L_3$ are both contributing to peak 9. $\Sigma_1(LA)\Sigma_4(TO)$, $L_3'L_1$, and combinations from the branches labeled A and B in Fig. 4 all the way from L to W have produced

peak 10. The four strong contributors to the hump 11 may also be seen in Table III. Thus these calculated features seem to be at least twice as strong as they should be, (and possibly even more when the three-phonon damping is included). The reason why the same features calculated by Berg and Bell are not as large is due mainly to the lower resolution obtained from their wave-vector grid.

In view of the comments above and in the subsection of Sec. II, the assignments made by Srivastava and Bist[4] may be seen to be incomplete, and erroneous. Furthermore, from an inspection of the data they obtained, the usefulness of the nujol mull technique in investigating these damping processes appears to be limited.

Note added in proof. While working with CsI, Beairsto and Eldridge (to be published in Can. J. Phys.) realized that no cubic coupling can occur through next-nearest-neighbor interactions, since they are ions of the same type. Coupling can occur through further opposite-type-neighbor interactions due to the long-range Coulombic terms and this will reduce the sharpness of the features calculated here. It was also found, however, that the next-nearest neighbors should be included in the repulsive component of the lattice potential energy.

ACKNOWLEDGMENTS

The authors would like to thank Dr. G. Dolling for the main routines of the shell-model program, and Dr. R. Howard for his assistance with that program. One of them (K.A.K.) would like to acknowledge the National Research Council of Canada for a 1 year graduate fellowship.

---

*Work supported by Grant No. A5653 from the National Research Council of Canada.

[1]J. E. Eldridge and Roger Howard, Phys. Rev. B 7, 4752 (1973).
[2]J. I. Berg and E. E. Bell, Phys. Rev. B **4**, 3572 (1971).
[3]J. E. Eldridge, Phys. Rev. B **6**, 3128 (1972).
[4]S. P. Srivastava and H. D. Bist, Phys. Status Solidi B **51**, 85 (1972).
[5]K. F. Renk, Phys. Lett. **21**, 132 (1966).
[6]G. Dolling, R. A. Cowley, C. Schittenhelm, and I. M. Thorson, Phys. Rev. **147**, 577 (1966).
[7]Note that for the parameters to be compatible with the program as described in Ref. 1, the electrical polarizabilities need to be divided by the volume of the unit cell in cm^3 times 10^{24}.
[8]R. P. Lowndes and D. H. Martin, Proc. R. Soc. A **308**, 473 (1969).
[9]A. M. Karo and J. R. Hardy, Phys. Rev. **129**, 2024 (1963).
[10]A. Savitsky and M. J. E. Golay, Anal. Chem. **36**, 1627 (1964).
[11]H. F. Macdonald, Miles V. Klein, and T. P. Martin, Phys. Rev. **177**, 1292 (1969).
[12]G. O. Jones, D. H. Martin, P. A. Mawer, and C. H. Perry, Proc. R. Soc. A **261**, 10 (1961).
[13]J. E. Eldridge, Phys. Rev. B **6**, 1510 (1972).
[14]I. G. Nolt, R. A. Westwig, R. W. Alexander, Jr., and A. J. Sievers, Phys. Rev. **157**, 730 (1967).
[15]A. Hadni, J. Claudel, G. Morlot, and P. Strimer, Appl. Opt. **7**, 161 (1968).
[16]K. D. Möller and W. E. Rothschild, *Far Infrared Spectroscopy* (Wiley, New York, 1971), p. 540.